BEHAVIOR OF MICROTREMOR H/V SPECTRUM AND PHASE VELOCITY ON THE BASIN PERIPHERAL AND INVERSION FOR DETERMINING BASIN STRUCTURE

H. Uebayashi[1], H. Kawabe[2], K.Kamae[3] and M.Horike[4]

[1] *Assoc. Prof.,* [4] *Prof., Dept. of Architectural Engineering ,Osaka Institute of Technology, Osaka.Japan*
[2] *Assist. Prof.,* [3] *Prof., Research Reactor Institute, Kyoto University, Osaka, Japan*
Email: uebayashi@archi.oit.ac.jp

ABSTRACT :

For expanding microtremor survey techniques to make it possible to estimate the irregular subsurface structure in sedimentary basins, the behavior of the H/V spectra and the phase velocities of microtremors on the basin periphery area was investigated to the southern Osaka basin. In the terrace area with a steep basement inclination, geophysical exploration methods on the basis of one-dimensional horizontally stratified model using microtremor phase velocity might have brought undesirable results. As the reason of the experimental results, it could be interpreted that microtremor array measurements are likely to be less 'robust' than microtremor H/V spectra measurements in a long period range. Therefore, the highly-accurate inversion analysis using microtremor H/V spectra was proposed as a tool for the modeling of the shape of basin-bedrock interface of basin structure based on numerical experiments.

KEYWORDS: Microtremors, H/V spectrum, Phase velocity, Irregular subsurface structure, Inversion

1. INTRODUCTION

The disaster belt generated during the 1995 Hyogo-ken Nanbu (Kobe) earthquake is caused with severe ground motions that were generated by a combination of forward directivity due to fault rupture and basin-edge amplification. This phenomenon implied that one of the key problems in strong motion predictions is the modeling of the shape of a basin-bedrock interface close to the basin peripheral. The microtremor survey is usefulness for estimating the basin structures because microtremor observation is simple, quake, and inexpensive. However, the reliability of subsurface structural models in the basin periphery estimated by the H/V spectra and/or the dispersion curves of microtremors is debatable because these features of microtremors are calculated by the characteristic equation of Rayleigh waves on the basis of a 1D horizontally stratified model. In the first part of this article, the behavior of H/V spectrum and phase velocity of microtremors is examined to the southern Osaka basin, called the Sen-nan Area. We conducted microtremor up-down component array observations and three-component single-station observations at 4 sites close to the locations of deep drilling for geophysical loggings or hot spring boring.

In many cases, modeling the shape of a basin-bedrock interface of a sedimentary basin using microtremor H/V spectra and phase velocities is performed by spatially arranging a 1D multi-layered structure to a subsurface structure located just under a surface observation point. Since such modeling techniques fail to take into account the effect of irregular subsurface structures on microtremor wavefields, the accuracy of these models may not be high in very irregular regions, such as areas located on a buried fault or at a basin edge (Uebayashi, 2003). The last part of this article presents a inverse analysis technique using microtremor H/V spectra for estimating the shape of 2D basin-bedrock interface of sedimentary basin.

2. BEHAVIOR OF H/V SPECTRUM AND PHASE VELOCITY ON THE BASIN PERIPHERAL

2.1. Basement structure obtained from the existing geophysical exploration results

Detailed basement structural models of the Osaka Basin have already been developed by the Geological Survey of Japan, AIST (2002) and Osaka Prefectural Government (2005). The model developed by Osaka Prefectural Government, which is shown in Fig.1, is the one with a partial improvement to the model developed by the

Geological Survey of Japan. Both models show that the density of highly reliable database of the basement depth obtained from a reflection survey and a down-hole survey is lower in Sennan District (the southern part of Osaka) than in Kobe District or Hokusetsu District. Therefore, the basement structure of Sennan District shown in Fig. 1 seems to be relatively less- accurate. Nevertheless, it can be geographically conjectured that the basement structural depth in Sennan District tends to increase gradually from south (Izumi mountainous area) to northwest (Osaka Bay). The sites with a circle (DH-A to D) plotted in Fig. 1 show the positions of down-holes excavated to the basement. DH-B and DH-C were drilled for hot spring boring, whereas DH-A and DH-D were drilled for geophysical logging. Drilling of DH-A was conducted by the National Research Institute for Earth Science and Disaster Prevention, and drilling of DH-D was recently conducted by Research Reactor Institute, Kyoto University. DH-A to C are located in the coastal area with a gentle basement inclination, while DH-D is located in the terrace area where the basement inclination is considered to be steeper.

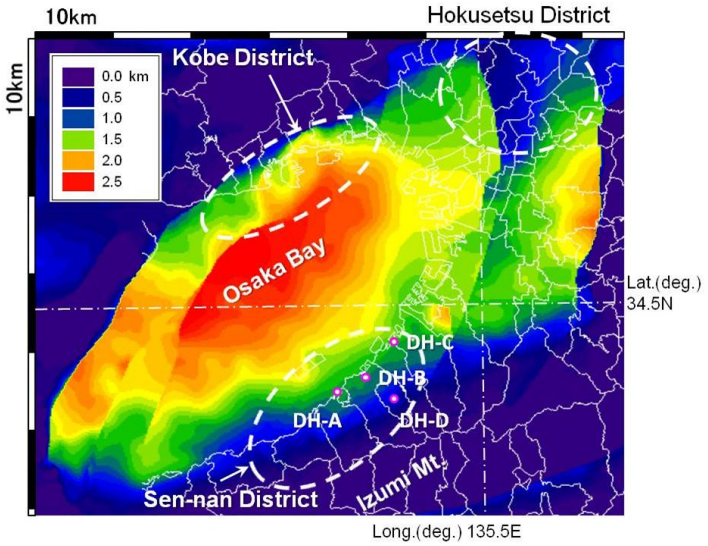

Figure 1. Contour map of the basement depth of Osaka basin and plots of investigated sites .

2.2. Comparison of S-wave velocity profiles based on various geophysical exploration methods

In recent years, geophysical exploration methods for obtaining the optimum velocity structure have been mainly employed, with a view to making the two characteristic curves of Rayleigh waves, namely, dispersion curves and ellipticity curves, correspond as much as possible to phase velocity and H/V spectra obtained from microtremor measurements, respectively. At the sites DH-A to D, where the basement depth was already obtained from a down-hole survey, the up-down component array measurements and three-component single-station measurements of microtremors were conducted. Then, the velocity profiles immediately below these sites were identified based on the fitting of the Rayleigh wave dispersion and ellipticity curves to the measurement results. Fig. 2 and Fig. 3 show dispersion curves and ellipticity curves of the identified subsurface structure at sites DH-A and DH-D, where velocity structure was obtained from geophysical exploration. In these figures, plots of phase velocity and H/V spectra obtained from the measurements are marked by red circles. The blue line in Fig. 2 shows the optimum solution obtained from inverse analysis of the dispersion curves, while the green line in Fig. 3 shows the optimum solution obtained from the inverse analysis of dominant frequency of ellipticity curves. In the inverse analysis of the dispersion curves, the subsurface structure was modeled as four layers. The SPAC method was employed to estimate phase velocity of Rayleigh waves obtained from the microtremor array measurement results. In the inverse analysis of the ellipticity curves, the geophysical parameters of the subsurface structure were modeled as a function of the depth, as in the above-mentioned Osaka Basin model. The following two results were obtained from these two inverse analyses: (1) In Fig. 2, except the frequency bands from 1.1 to 1.3HZ shown in Fig. 2 (b), the blue line agrees well with the red circles; and, (2) In Fig. 3, dominant frequencies marked by the green line and the red circles show a good agreement. This also suggests that dispersion curves and ellipticity curves calculated by the velocity structure profiles identified in the two inversion analyses agree well at DH-A (Fig.2(a), Fig.3(a)), while they are obviously different at DH-D (Fig.2(b), Fig.3(b)).

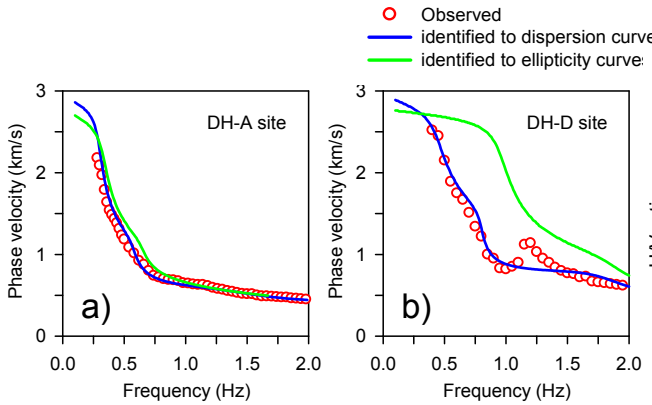

Figure 2. Dispersion curves of the identified structures.

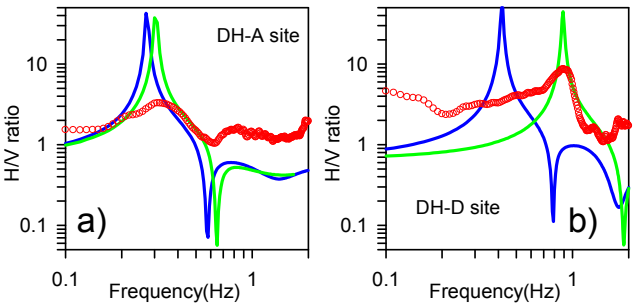

Figure 3. Ellipticity curves of the identified structures.

Fig. 4 shows the comparison of the S-wave velocity profiles obtained from down-hole logging and S-wave velocity profiles identified by the above-mentioned two microtremor exploration methods at DH-A and DH-D. As shown in Fig.4 (a), the three profiles are in good agreement at the basement and sedimentary layer at DH-A. Table 1 shows the basement depth obtained using three different methods at four sites. At DH-B and DH-C, the basement depths obtained by down-hole logging are close to those obtained from the two microtremor exploration methods. This means that in the coastal area with a gentle basement inclination, the two microtremor exploration methods would give the appropriate basement depth. On the other hand, as shown in Fig. 4 (b), the basement depth obtained from ellipticity curves shows an agreement with the one obtained from the down-hole S-wave logging. However, the basement depth obtained from dispersion curves marked with a blue line is about three times as deep as the one obtained from the down-hole S-wave logging marked with a red line. According to the authors' experiences in conducting microtremor geological exploration, phase velocity based on microtremor array measurements in a long period range tends to have more errors than microtremor H/V spectra. Based on such experiences and analytical results in this paper, it can be interpreted that microtremor array measurements are likely to be less 'robust' than microtremor H/V spectra measurements in a long period range. Therefore, it is considered that in the terrace area with a steep basement inclination, geophysical exploration methods using microtremor phase velocity might have brought undesirable results. Moreover, as Uebayashi (2003) has reported, in the three-dimensionally complicated subsurface structural region, the dominant frequencies of microtremor H/V spectra do not agree with those of ellipticity curves of Rayleigh wave. This indicates that in the highly-accurate inversion analysis of irregular subsurface structures, it is necessary to take into account two- or three-dimensional scattered wave fields when modeling.

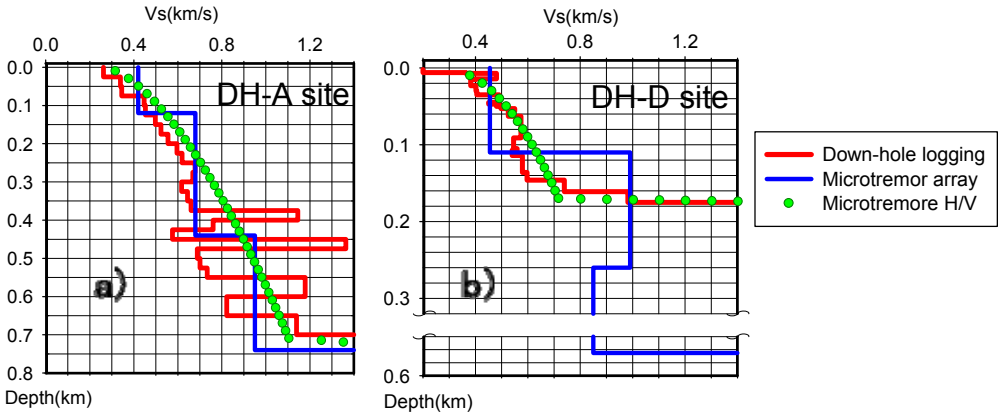

Figure 4. Comparison of the S-wave velocity profiles obtained from down-hole logging and identified by two microtremor explorations.

Table 1. Basement depths obtained using three different methods at four sites

	DH-A	DH-B	DH-C	DH-D
Down-hole	700 (m)	811	1064	184
Phase velocity	735	810	1000	530
H/V spectra	726	821	983	174

3. INVERSION PROCEDURE FOR DETERMINING BONDARY SHAPE OF BASIN STRUCTURE

3.1. Finite element model and incident waves

Forward analysis of waves propagating through a 2D basin structure was performed using the frequency-domain finite element method. A basin-bedrock interface buried in a square area containing a sedimentary layer was searched for using fine grids as shown in the lower part of Fig. 5. The minimum grid size is determined by two conditions, namely the required spatial resolution and the minimum wavelength of the S waves. The basement region is subdivided into course grids and a viscous boundary condition is defined for the base of the region and an energy-transfer boundary condition is defined for each of the two sides.

Since this paper is concerned with long-periods ranging from 1 to 10 seconds, the source of microseisms can be assumed to be the pressure variation at the seabed produced by waves on the surface of the ocean (Longuet-Higgins, 1950). Uebayashi (2003) demonstrated that this assumption is valid by comparing the microseism power spectra of a sedimentary layer and the spectra of significant ocean wave height over time. As the lower part of Fig.5 shows, the incident fundamental Rayleigh waves from outside the sedimentary basin to the left and right of the basement region have the same amplitude. The transfer functions for these input ground motions are then calculated at the observation points on the sedimentary layer. Horizontal-to-vertical spectra are obtained from the ratios of the absolute horizontal and vertical components of the transfer functions.

For the inverse analysis algorithm, we selected a genetic algorithm (GA) since it is considered to be effective for searching for a global minimum optimal solution. If a large search space of a basin structure is used, many steps of conversion computation are generally necessary to obtain a good optimal solution requiring a long computation time. In order to efficiently search for the optimal solution at a high resolution, the basin region was split into a models having a hierarchy of grid sizes and several horizontal submodels.

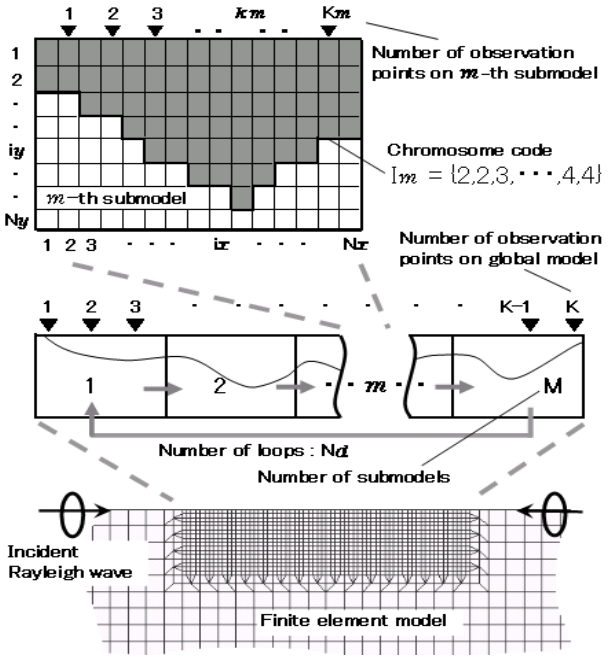

Figure 5. Configuration of a basin structure divided into several submodels and the depth of an irregular interface encoded by a sequence of natural numbers.

3.2. Inversion procedure applying genetic algorithm

3.2.1. Grid-size hierarchical models

A high resolution solution is found by hierarchicalization, that is by searching for approximate solutions for the depth of the basin-bedrock interface using coarse grids and then obtaining an optimum solution by gradually reducing the grid size. Since the number of vertical grids increases and the solution search range is extended as the number of hierarchical levels increases, we imposed the condition of setting the depth of the basin-bedrock interface of the initial model for each hierarchy ± 2 grids as the upper and the lower limits for the search range. Extending the target frequency band of the inverse analysis in proportion to the hierarchy size will make the misfit curved surface smooth and avoid placing a constraint on the local minimum.

3.2.2. Horizontal submodels

The frequency characteristics of microseism and seismic H/V spectra in a sedimentary layer proved to be suitable for an irregular subsurface structure area (Zhao et al., 1997). This finding suggests that H/V spectra are insensitive to the origin and the propagation path but are sensitive to the subsurface structure located near the observation point. As the central section of Fig.5 shows, the global model for a sedimentary basin is divided into several (M) submodels arranged horizontally. Inverse analysis is then performed on each submodel in order. The other submodels are fixed at the optimal solution obtained in the preceding step. The submodels are then updated sequentially as the optimal solutions obtained for each submodel become the new values. After inverse analysis has been performed on all of the M models, the submodels are re-analyzed starting with the first one. This is repeated a specified number (Nd) of times.

The chromosome codes Im (see the upper part of Fig.5) of the individuals in the m-th submodel are expressed by a row of natural numbers. The submodel is equally divided into Nx grids in the horizontal direction and Ny grids in the vertical direction. The grid size is D. The locus represents the horizontal grid position ix and its position (gene) represents the vertical number of grids iy which corresponds to the depth of the basin-bedrock interface. If the lower limit of the search range is set to D×Ny using a priori information on the basement depth obtained from past surface geology studies and explorations of the subsoil, the possible range of the gene will be $0 \leqq iy \leqq Ny$.

The number of submodels M is varied hierarchically. If the submodel width is small, the search range will be narrow. If, however, the H/V spectra are influenced by scattered waves from a subsurface structure located outside the target submodel, it will not be possible to obtain an accurate solution in this case. If the width is large, the search range will be wide and it will take a long time to find the optimal solution. Thus, there exists a tradeoff between the submodel width and the search performance. We investigated in previous paper (Uebayashi, 2006b) how the scattered wave from the submodels outside the target submodel will affect the H/V spectra at the observation point located at the center of the target submodel.

3.3. Setting of genetic algorithm parameters

We used both expected value and elite preservation strategies as GAs in this study. The probability of crossover was set to 0.6 and the crossover type was a two-point crossover. The probability of mutation changes dynamically until the number of generations n_g equals Ng_0. When the number of generations n_g satisfies the condition $0<n_g \leqq Ng_0$, the probability increases from 0.01 to 0.05 in proportion with the number of generations but remains constant at 0.05 when $n_g \geqq Ng_0$. From data regarding the deposition process of the layer, the shape of the basin-bedrock interface is considered to vary smoothly over a wide area of the sedimentary basin. Thus, to 60% of individuals in an individual group, we applied a spatial weighted mean, namely a Hanning-window digital filter having a value for the individual Im representing the depth distribution of the basin-bedrock interface. The number of grids iy(ix) at position ix is computed from iy(ix)=0.15iy(ix-1)+0.7iy(ix)+0.15iy(ix+1). Inverse analysis is repeated on a submodel up to the fixed generation Ng and the individual having the maximum fitness value described in the following section becomes the solution to the m-th submodel. This operation is repeated over a double loop on m and n_d and the submodel solution is updated sequentially. Therefore, the total number of generations Ng^{total} in a hierarchy can be expressed as follows:

$$Ng^{total} = Ng \times M \times Nd \tag{3.1}$$

The optimum global model of $\{I_G\}=\{I_1, I_2, \ldots, I_M\}$ obtained in this hierarchy becomes the initial value for the next hierarchy.

3.4. Residual evaluation function of H/V spectra

The H/V spectra at observation points (1,2 … ,k_m, … ,K_m) on the m-th submodel at the upper part of Fig.5 are computed for the subsurface structure model corresponding to individual j (j=1,2, …J, J: number of individuals). Then the reciprocal of the misfit of the H/V spectra is computed as a mean about the target frequency. We calculate this reciprocal at each observation point and formulate the fitness function $F_{m,j}$ equivalent to the objective function that is a spatial weighted mean.

$$F_{m,j} = \sum_{km=1}^{Km} \frac{w_{km}}{\frac{1}{Nf}\sum_{\ell=1}^{Nf}\left(\frac{HV_{\ell,km}^{target} - {}_jHV_{\ell,km}^{trial}}{HV_{\ell,km}^{target}}\right)^2} \quad \text{where} \quad \sum_{km=1}^{Km} w_{km} \fallingdotseq 1 \tag{3.2}$$

where w_{km} is the spatial weighted function at the km-th observation point and has as a normal distribution probability density function N (mean k_m=Nx/2, standard deviation σ=0.6) and where N_f is the maximum value of the discrete target frequency. The impact of the number of observation points on the robustness of an estimated solution was checked in Uebayashi (2006b). As the result, we reached the conclusion that increasing the number of observation points will not improve the efficiency of inverse analysis if the distance between observation points is about a half the minimum wavelength of S-waves at the target upper frequency limit.

4. VERIFICATION BY NUMERICAL EXPERIMENTS

Table 2 gives the values of the geophysical parameters of the sedimentary basin model used in the numerical experiments. The parameters of the sedimentary layer generally changes with depth. However, the search space is extended if a multilayer structure model is created with the sedimentary layer composed of curved interfaces and added to inverse analysis as a variable-like basin-bedrock interface. An enormous volume of computation is required to obtain an accurate optimal solution using the previously described algorithm. To prevent extending the search space, we assigned functions that were dependent on depth to the geophysical parameters of the sedimentary layer in this study. Table 3 gives parameters related to the inverse analysis. The number of hierarchies was set to three. These parameters were assigned on the basis of numeric values obtained by thorough investigation by Uebayashi (2006a). Figure 6 compares the depth distribution of the basin-bedrock interface between the evaluated model and the target model for each hierarchy level. Based on the results of the numerical experiments mentioned in the previous paper (Uebayashi, 2006b), the total number of observation points K was set to 27. The right side of each figure shows the S-wave velocity profile as a function of depth of

Table 2. Geophysical parameters of the structure models.

	Vp(km/s)	Vs(km/s)	Density(g/cm^3)	Q_s
Sediment	1.45+0.31d	0.60+0.47d	1.00+0.52d	30
Bedrock	3.0	5.4	2.5	100

d is depth(km).

Table 3. Parameters used to invert each hierarchical models.

Hierarchy	Frequency band (Hz)	Resolution (D)	Submodel (M)	Loop (N_d)	Generation (Ng)
Low	Δf ～0.275Hz	0.60km	2	3	75
Intermediate	Δf ～0.425Hz	0.30km	3	3	50
High	Δf ～0.750Hz	0.15km	4	3	40

Δf = 1/102.4(Hz)

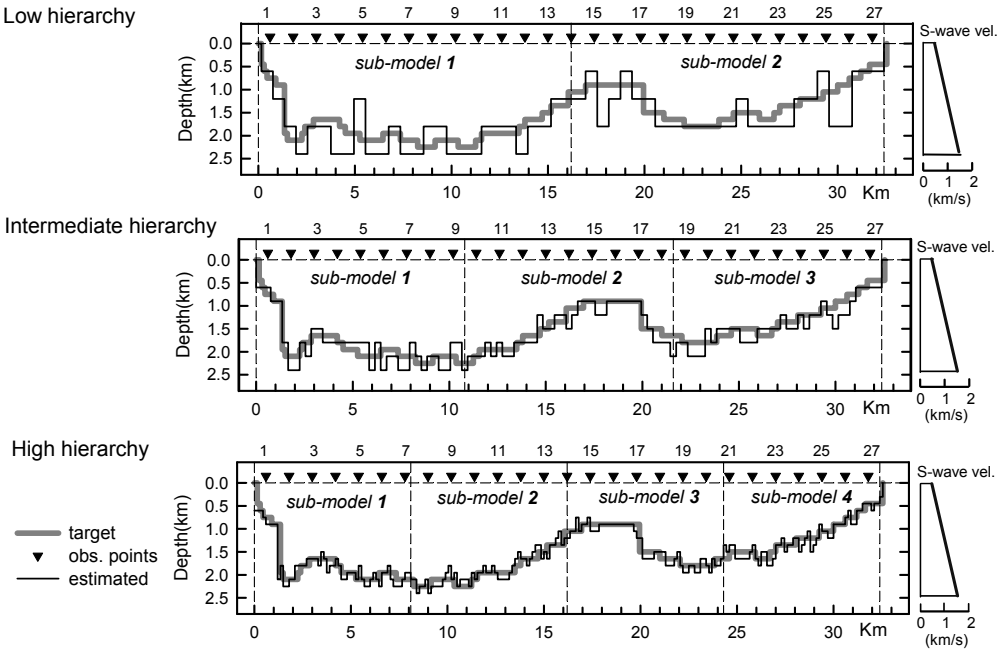

Figure 6. Comparison of the basin structures between the target and estimated models.

the sedimentary layer. The bold gray line represents the target value while the fine black line represents the estimated result. Comparing these two lines, we see that the residual difference decreases as the level of hierarchy increases. Even at the joints between submodels represented by broken lines in the figure the basin-bedrock interface changes smoothly, indicating good agreement with the target value.

Figure 7 shows the variation in the residual difference with the number of grids as a function of the generation number of the inverse analysis process until the optimal solution shown in Fig.6 is achieved. For all three levels of hierarchy, the residual difference of the depth of the basin-bedrock interface is given in units of the minimum grid size (D = 0.15 km). The bold solid line represents the mean and the standard deviation of the grid residual difference for a group consisting of 20 individuals (j=1,2, … ,20). The fine solid line represents the generation changes of the residual differences about the individuals of the optimal solutions shown in Fig.6 (indicated by arrows). We used the formula of the fitness function mentioned previously as an index to evaluate the accuracy of the solution. According to Uebayashi (2006a), the value is maximized for the individual that approximately corresponds to the model of the minimum residual difference in the number of grids. The generation changes has the tendency that the residual difference decreases more rapidly in the initial generation since the hierarchy level is lower. This is probably because the grids are larger in lower hierarchies and the initial generation converges faster to the local minimum that is a characteristic of GA.

Figure 8 shows the H/V spectra at the major observation points of the ones shown in Fig.6. At any observation point, the bold gray line represents the target and the circles indicates the estimated result and there is good agreement between them even in the high frequency range.

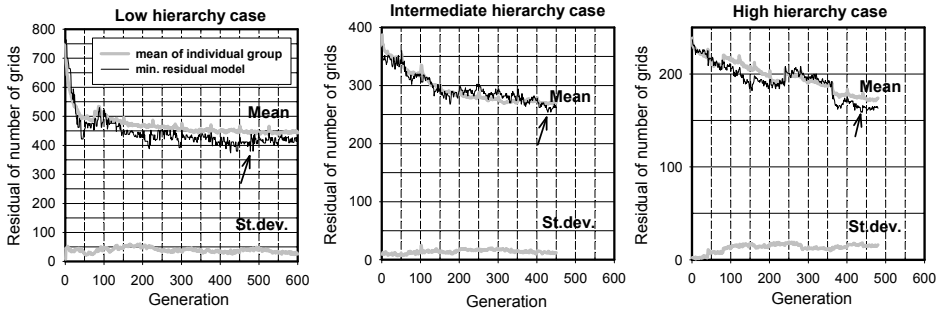

Figure 7. Changes in residuals of number of grids over generations for each step of the hierarchy..

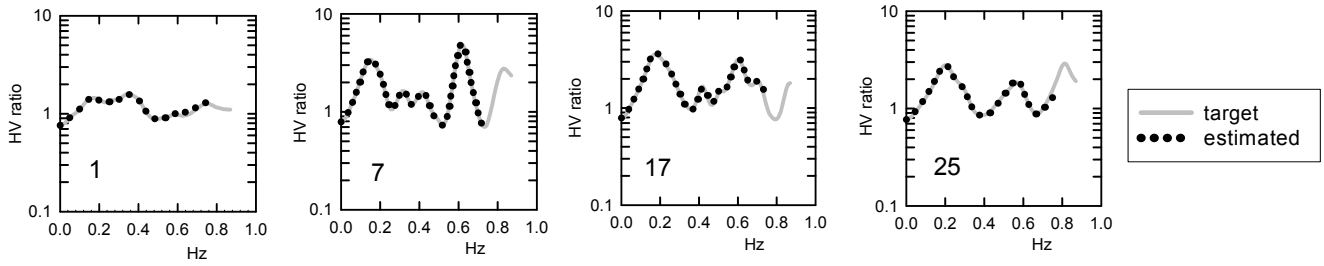

Figure 8. Comparison of H/V spectra between the target and estimated models

.

5. CONCLUSIONS

The two microtremor features, namely, the H/V spectra and the phase velocities, on the basin periphery area were investigated to the southern Osaka basin. In the coastal area with a gentle basement inclination, the S-wave velocity profile identified from the two features gave the appropriate basement depth. On the other hand, in the terrace area with a steep basement inclination, the S-wave velocity profile identified from the phase velocity was quite different from the one obtained from the down-hole S-wave logging. As the reason of the experimental results, it could be interpreted that microtremor array measurements are likely to be less 'robust' than microtremor H/V spectra measurements in a long period range.

To estimate the depth of the basin-bedrock interface in a sedimentary basin, we proposed an effective inverse analysis technique that applies the GA to microseism H/V spectra. The results are summarized below. By combining the two techniques mentioned below we were able to achieve both high resolution and high search efficiency. The two techniques employed were, 1) making grids hierarchical and setting constraints on the upper and lower limits of the depth of basin-bedrock interface for the search, and 2) dividing an entire basin structure into submodels.

REFERENCES

Longuet-Higgins, M. S. (1950), A theory of the origin of microseisms, Phil. Trans., Roy. Soc. London A243,1-35.

Uebayashi H. (2003), Extrapolation of irregular subsurface structures using the horizontal-to-vertical spectral ratio of long-period microtremors, Bullitin of Seismological Society of America, Vol.93, 570-582.

Uebayashi, H. (2006a), Inversion of microseism horizontal-to-vertical spectral ratio for determining the boundary shape of a basin structure, Journal of Structural and Construction Engineering, Transactions of Architectural Institute of Japan, No.603 May, 69-76 (in Japanese with English abstract and figure's captions).

Uebayashi, H. (2006b), Inversion of microseisms horizontal-to-vertical spectral ratio for determining the boundary shape of basin structure based on numerical experiments, 3rd International Symposium on the ESG,

Osaka Prefectural Government (2005), Contract report concerning subsurface structure investigation of Osaka plains (in Japanese).

Horikawa H., Mizuno K., Satake K., Sekiguchi H., Kase Y., Sugiyama Y., Yokota H., Suehiro M. and Pitarka A. (2002), Three-dimensional subsurface structure model beneath the Osaka plain, Geological Survey of Japan, National Institute of Advanced Industrial Science and Technology, Vol.2, 291-324 (in Japanese).

Zhao B., Horike M., Takeuchi Y. and Kawase H. (1997), Comparison of site-specific response characteristics inferred from seismic motions and mincrotremors, Zisin; Journal of Seismological Society of Japan, Vol.50-1, 67-87 (in Japanese with English abstract).

National Research Institute for Earth Science and Disaster Prevention (since 2000), Digital strong-motion seismograph network KiK-net, http://www.kik.bosai.go.jp/kik/ftppub/sitepdf/OSKH01-E.pdf

Acknowledgments

We are grateful to Dr. Ken Miyakoshi of Geo-research institute and Mr. Koji Yamada of Hanshin Consultants Co., LTD for offering of the geological information of the Osaka basin. This study was supported in part by Grant-in-Aid for Scientific Research (No.20560540) from Japan Society of the Promotion Science.